



HAL
open science

NIR-II Aza-BODIPY Dyes Bioconjugated to Monoclonal Antibody Trastuzumab for Selective Imaging of HER2-Positive Ovarian Cancer

Amélie Godard, Ghadir Kalot, Malorie Privat, Mohamed Bendellaa, Benoit Busser, K. David Wegner, Franck Denat, Xavier Le Guével, Jean-Luc Coll, Catherine Paul, et al.

► **To cite this version:**

Amélie Godard, Ghadir Kalot, Malorie Privat, Mohamed Bendellaa, Benoit Busser, et al.. NIR-II Aza-BODIPY Dyes Bioconjugated to Monoclonal Antibody Trastuzumab for Selective Imaging of HER2-Positive Ovarian Cancer. *Journal of Medicinal Chemistry*, 2023, 66 (7), pp.5185-5195. 10.1021/acs.jmedchem.3c00100 . hal-04091996

HAL Id: hal-04091996

<https://hal.science/hal-04091996>

Submitted on 9 May 2023

HAL is a multi-disciplinary open access archive for the deposit and dissemination of scientific research documents, whether they are published or not. The documents may come from teaching and research institutions in France or abroad, or from public or private research centers.

L'archive ouverte pluridisciplinaire **HAL**, est destinée au dépôt et à la diffusion de documents scientifiques de niveau recherche, publiés ou non, émanant des établissements d'enseignement et de recherche français ou étrangers, des laboratoires publics ou privés.

NIR-II aza-BODIPY dyes bioconjugated to monoclonal antibody trastuzumab for selective imaging of HER2-positive ovarian cancer

Amélie Godard^{1*} & Ghadir Kalot^{2*}, Malorie Privat^{1,3,4}, Mohamed Bendellaa², Benoit Busser^{2,5,6}, K. David Wegner⁷, Franck Denat¹, Xavier Le Guével², Jean-Luc Coll², Catherine Paul^{3,4}, Ewen Bodio¹, Christine Goze^{1*®} & Lucie Sancey^{2*®}

¹ Institut de Chimie Moléculaire de l'Université de Bourgogne, Université de Bourgogne, CNRS UMR 6302, 21078 Dijon, France.

² Université Grenoble Alpes, INSERM U1209, CNRS UMR 5309, Institute for Advanced Biosciences (IAB), 38000 Grenoble, France.

³ Laboratoire d'Immunologie et Immunothérapie des Cancers, EPHE, PSL Research University, 75000 Paris, France.

⁴ LIIC, EA7269, Université de Bourgogne, 21000 Dijon, France.

⁵ Grenoble Alpes University Hospital (CHUGA), 38043 Grenoble, France.

⁶ Institut Universitaire de France (IUF) 75005 Paris, France.

⁷ Division Biophotonics, Federal Institute for Materials Research and Testing (BAM), 12489 Berlin, Germany.

@ E-mail: christine.goze@u-bourgogne.fr; Lucie.sancey@univ-grenoble-alpes.fr

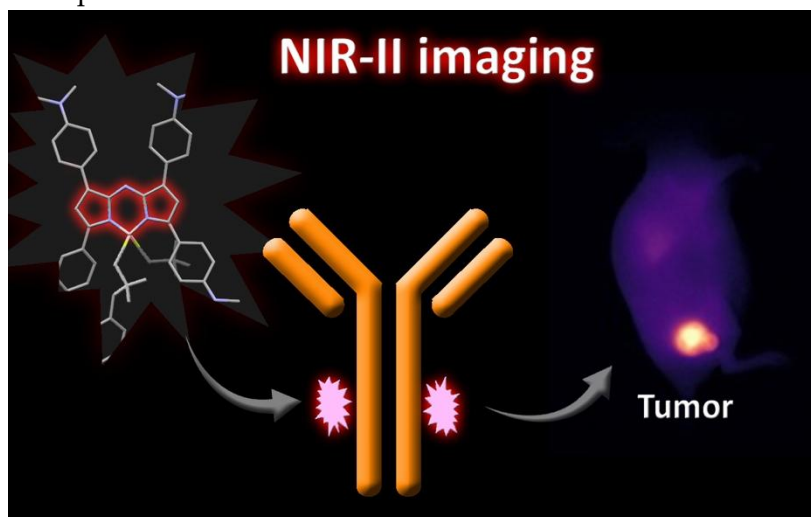
* Equal contribution

Abstract:

Using fluorescence guided surgery (FGS) to cytoreductive surgery helps achieving complete resection of microscopic ovarian tumors. The use of visible and NIR-I fluorophores has led to beneficial results in clinical trials; however, involving NIR-II dyes seems to outperform those benefits due to the deeper tissue imaging and higher signal/noise ratio attained within the NIR-II optical window. In this context, we developed NIR-II emitting dyes targeting HER2-positive ovarian tumors, by coupling water-soluble NIR-II aza-BODIPY dyes to the FDA approved anti-HER2 antibody, namely trastuzumab. These bioconjugated NIR-II-emitting dyes displayed a prolonged stability in serum, and a maintained affinity towards HER2 *in vitro*. We obtained selective targeting of HER2 positive tumors (SKOV-3) *in vivo*, with a favorable tumor accumulation. We demonstrated the fluorescence properties and the specific HER2 binding of the bioconjugated dyes *in vivo*, and thus their potential for NIR-II FGS in the cancer setting.

Keywords: aza-BODIPY, NIR-II imaging, bioconjugated dye, site-specific bioconjugation, ovarian cancer, HER2.

Table of Contents Graphic:



Introduction:

Ovarian cancer is the most lethal gynecologic cancer, with 75% of patients being diagnosed at advanced or late stages, and 5-year relative survival being under 50% ¹. The typical standard of care consists in performing cytoreductive surgery followed by platinum-based chemotherapy. Depending on the surgeon's visual inspection and palpation during surgery, cytoreductive surgery allows the resection of large and visible tumors. However, the identification of microscopic lesions remains challenging, even for skilled surgeons. Those residual tumors are considered as an important predictor of survival, with a 5.5% increase in the median survival achieved for each 10% increase in optimal cytoreduction ², with patients undergoing complete or optimal cytoreduction (resected tumor size = 1-10 mm) showing improved overall survival as compared to patients undergoing suboptimal cytoreduction (resected tumor size > 10 mm) ³. With the aim of reducing mortality, the ultimate goal is to optimize surgical procedures to achieve complete resections.

To this end, fluorescence guided surgery, a safe (non-ionizing), inexpensive, sensitive and real-time intraoperative molecular imaging technique, was introduced into clinical practice ⁴. Fluorescence guided surgery (FGS) is based on the use of a fluorophore, alone or coupled to a targeting moiety, that labels for example cancer cells to improve their detectability *versus* healthy tissues, thus increasing the complete resection rate. Among the fluorophores developed for tumor imaging and in particular for FGS, some of them are emitting in the visible range ⁵, and other fluorophores are emitting in the NIR region (700-900 nm) ⁶.

In the last couple of years, the NIR-II optical window (1000-1700 nm, also called SWIR for ShortWave Infrared) caught increasing attention due to its even reduced tissue autofluorescence and less photon scattering as compared to NIR-I, with higher light penetration depths,

improved signal-to-noise ratios and high-resolution images ⁷. In this context, many NIR-II fluorophores have been reported in the literature. Some of them may present potential toxicity due to their chemical composition as QDots⁸, or are difficult to bioconjugate efficiently⁹. Interesting results have been obtained with organic compounds bioconjugated to peptides¹⁰, but few compounds are reported to have a photostable NIR-II emission with a favorable quantum yield, while coupled to antibodies¹¹. In parallel, we recently developed a NIR-II emitting fluorophore based on aza-BODIPY platform named **SWIR-WAZABY-01** ¹². As other aza-BODIPYs, this dye possesses an excellent photostability ¹³. Its NIR-II emission properties, and water-solubility favored its use for biological applications, in particular for *in vivo* tumor imaging ¹². Following intravenous administration, **SWIR-WAZABY-01** is transported in the bloodstream *via* natural lipoproteins, enabling the specific labeling of tumors overexpressing lipoprotein receptors, LDLR and SR-BI, namely LDL receptor and Class B Scavenger receptor B1, respectively. The NIR-II emitting dye accumulated significantly in the tumor area in the absence of any targeting moiety ¹⁴. In order to benefit from **SWIR-WAZABY-01** unique NIR-II photophysical properties and to target ovarian tumors regardless of their lipoprotein receptors expression profiles, we coupled this NIR-II emitting dye to trastuzumab, an antibody specific to HER2 (human epidermal growth factor receptor 2) which is overexpressed in several tumor types including ovarian tumors ¹⁵.

In this study, we report the development of a NIR-II dye targeting HER2-positive ovarian cancer (**aza-SWIR-trastuzumab-01**), based on the water-soluble aza-BODIPY dye **SWIR-WAZABY-01** conjugated to trastuzumab antibody. A specific bioconjugation process was applied, resulting in a stable cancer targeting dye with a maintained affinity for HER2, both in solution and *in vitro*. *In vivo*, **aza-SWIR-trastuzumab-01** showed a high selectivity to ovarian cancer expressing HER2, which was not the case for non-targeted fluorophore **SWIR-WAZABY-01**. To increase the optical properties of the dye, another bioconjugate - **aza-SWIR-trastuzumab-02** - based on a brighter water-soluble aza-BODIPY dye - **SWIR-WAZABY-02** - conjugated to trastuzumab antibody, was also synthesized. Compared to **aza-SWIR-trastuzumab-01**, **aza-SWIR-trastuzumab-02** showed an important tumor/muscle ratio, superior to those reported in the literature for optical imaging ¹⁶.

Results and discussion:

Chemical synthesis

For a selective targeting, we coupled the **SWIR-WAZABY-01** to the monoclonal antibody trastuzumab. Indeed, the high and prolonged photo- and chemical stabilities of **SWIR-WAZABY-01**^{12, 14} made it compatible with the slow biodistribution of the antibodies. To carry out the proof-of-concept of targeted tumor imaging in the NIR-II region, we worked with two types of bioconjugation: i) a random bioconjugation, based on the reaction between the dye and the amino group available on the different free lysins of the trastuzumab antibody, and ii) a site-specific bioconjugation, which allows tethering the dye to the modified oligosaccharide chains (Fc part) of the antibody (*Figure 1a*). The **SWIR-WAZABY-01** precursor (*i.e.* compound **aza-propargyl-01**) was modified in order to add a grafting function on the dye to perform the different bioconjugations (*Scheme S1* and *Figures S1-S6*).

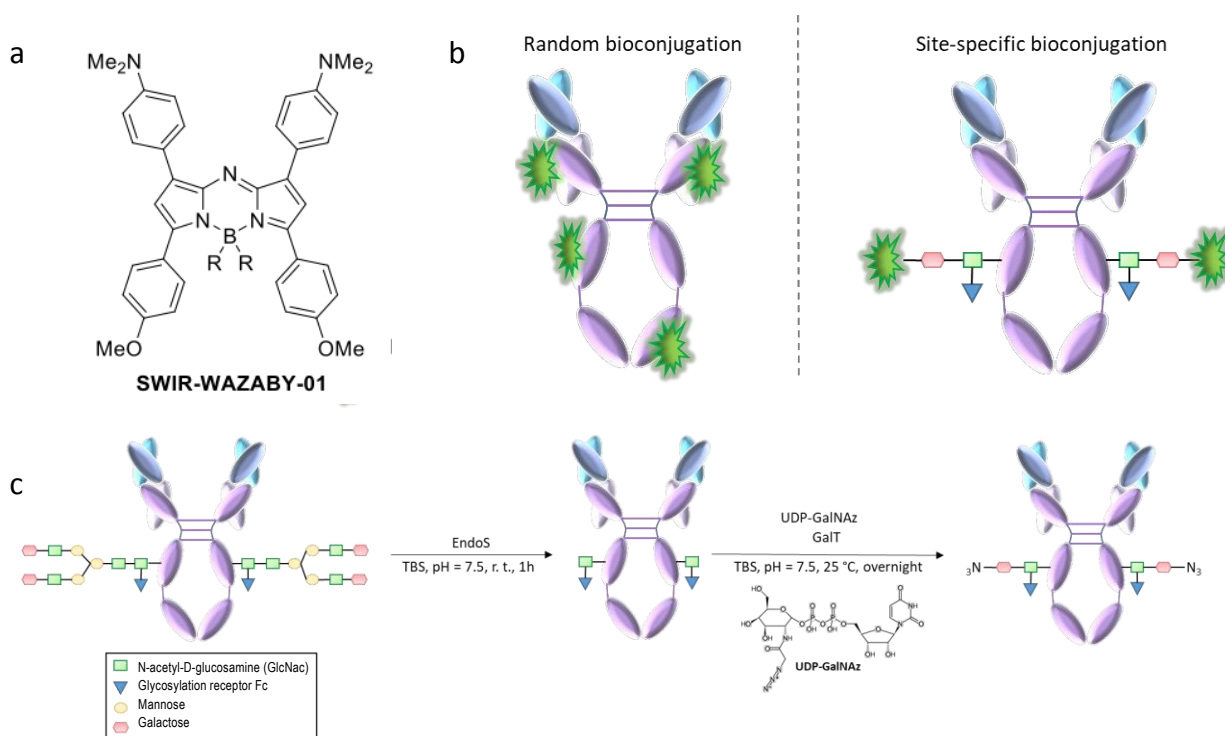


Figure 1: (a) Chemical structure of SWIR-WAZABY-01. (b) Schematic representation of the grafting of a dye on trastuzumab antibody using random bioconjugation (left) and specific bioconjugation with GlyCLICK® kit (right). (c) Schematic representation of the modification of trastuzumab antibody using GlyCLICK®.

The goal of the synthesis was the grafting of a TOTA (4,7,10-trioxa-13-tridecanamine) group on compound **aza-propargyl-01** in two steps. The compound **aza-propargyl-01** and 4-bromomethylbenzoic acid were solubilized in THF and refluxed overnight to isolate **aza-acid-01** in 22% yield. Following a peptidic coupling in presence of HBTU, **aza-acid-01** reacted with

TOTA-Boc at 30 °C for 1.5 h in DMF in basic medium. The quaternization of the remaining amine was performed using an excess of iodomethane in DCM followed by a deprotection step to isolate **aza-TOTA-01** in 15% yield, after a semi-preparative HPLC purification.

For the random bioconjugation (*Figure 1a left*), **aza-TOTA-01** was modified by adding a squaramate group to get **aza-squaramate-01** in 83% yield. This dye was incubated with trastuzumab in bicarbonate buffer (pH = 8.9) to obtain a degree of labeling (DOL) of 2 (*i.e.* two dyes grafted per antibody). A DOL of around 2 enables to prevent any fluorescence signal quenching, preserves the antibody's affinity towards HER-2, and limits the impact on the antibody's distribution¹⁷. Two parameters were modified for the bioconjugation: the time of reaction and the number of equivalents of **aza-squaramate-01** used. Unfortunately, despite the various attempts, only a few dyes were effectively grafted (DOL < 1), this is why the bioconjugation was then performed in a site-specific way.

For the specific bioconjugation (*Figure 1a right*), a constrained cyclic alkyne group was introduced onto **aza-TOTA-01** *via* a constrained cycle BCN (bicyclo[6.1.0]nonyne) to lead to **aza-BCN-01** in 56% yield. The site-specific bioconjugation allowed to obtain a DOL around 2, reproducibly. To this end, the trastuzumab antibody was modified with two azide functions, enabling the reaction with **aza-BNC-01** *via* a strain-promoted alkyne-azide cycloaddition (SPAAC) (copper-free click-chemistry)¹⁸. Azides were introduced onto the oligosaccharide chain of the antibody Fc part using GlyCLICK® technology based on two enzymes (*Figure 1b*). First, the EndoS hydrolyzed the binding between two *N*-acetylglucosamines resulting in a deglycosylated trastuzumab. Then, the GalT ensured the transfer of an azide-bound galactose from UDP-GalNaz to the deglycosylated antibody, generating the trastuzumab-N₃. Trastuzumab-N₃ was incubated with 15 equivalents of **aza-BCN-01** in phosphate buffer (PBS, pH = 7.4) overnight, and purified by fast protein liquid chromatography (FPLC). The purified **aza-SWIR-trastuzumab-01** was concentrated, and the trastuzumab's degree of labeling (DOL) was determined using MALDI-TOF mass spectrometry analyses. A DOL of 1.9 dyes per antibody was obtained (*Figure S7a*).

Stability and specificity

The fluorescence stability of **aza-SWIR-trastuzumab-01** was assessed at 37 °C in the presence of murine serum at different timepoints (0, 24, 48, and 72 h) to mimic *in vivo* conditions (*Figure 2*). The incubated mixtures were then separated on a polyacrylamide gel under native and reductive conditions (in presence of DTT and heating to 95 °C), followed by fluorescence image analysis (according to previously reported procedure¹⁹). As expected, no fluorescence was detected for non-labeled trastuzumab antibodies. Concerning **aza-SWIR-trastuzumab-01**, under native conditions, a single fluorescent band was observed at the position ~ 150 kDa, which corresponds to the size of the full trastuzumab antibody²⁰. No evolution or decline in the fluorescence signal was observed after 72 h of incubation, indicating the stability of the

bioconjugate under murine physiological conditions. Under reducing conditions, the disulfide bridges connecting the heavy and light chains of the antibody are broken, and we observed the fluorescence bands at lower molecular weights (~ 50 kDa), corresponding to the approximate weight of antibody's heavy chains²⁰. No fluorescence was observed at the light chain position (~ 25 kDa)²⁰. These data confirm that the dye was specifically grafted on the antibody heavy (Fc) chain. Similar data were also obtained when the incubation was performed with human serum (*Figure S8*).

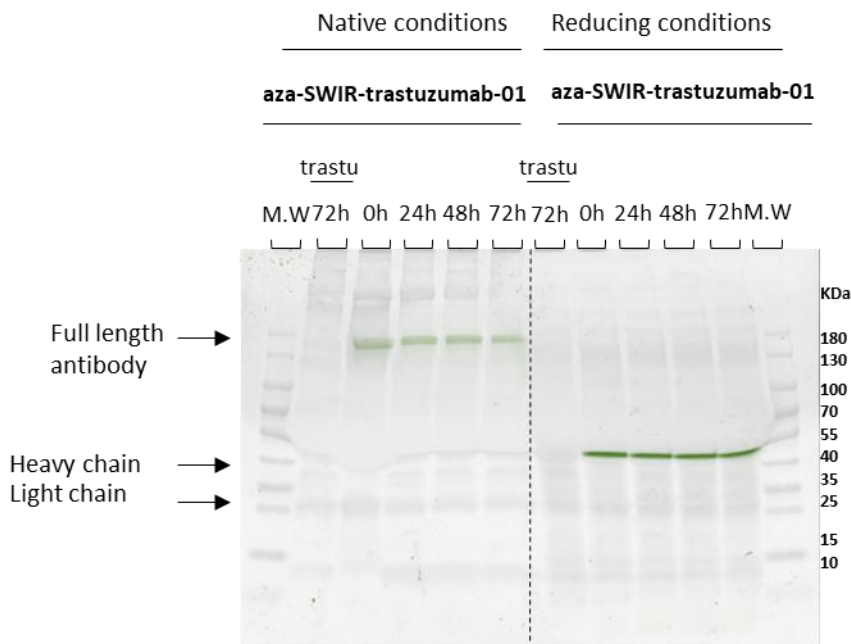


Figure 2: Assessment of aza-SWIR-trastuzumab-01 stability in murine serum solution. Superimposed fluorescence image (in green) and bright field image of **aza-SWIR-trastuzumab-01** + serum mixture migration on SDS-PAGE gel, under native and reducing conditions (DTT + heating). **Aza-SWIR-trastuzumab-01** was incubated in murine sera for 0, 24, 48 and 72 h. Free trastuzumab (non-fluorescent, trastu) incubated with serum for 72 h, served as a control.

To assess whether the fluorophore grafting steps altered the affinity of trastuzumab towards its target (HER2), a biolayer interferometry experiment was performed²¹. This experiment allowed the study of the association/dissociation dynamics of **aza-SWIR-trastuzumab-01** with HER2 protein (*Figure 3b*). Accordingly, the affinity of **aza-SWIR-trastuzumab-01** for HER2 (K_D) was calculated (*Figure 3c*). Using similar experimental conditions, the affinity of trastuzumab for HER2 (K_D) was calculated and served as a control (*Figure 3a,c*). The K_D of **aza-SWIR-trastuzumab-01** ($K_D = 9.5 \text{ nM} \pm 2.5 \text{ nM}$) was only slightly altered compared to that of native trastuzumab ($K_D = 4.8 \text{ nM} \pm 1.8 \text{ nM}$), indicating that the applied bioconjugation resulted in the **aza-SWIR-trastuzumab-01** product with a conserved affinity for HER2.

For confirmation, the targeting capacity of the **aza-SWIR-trastuzumab-01** towards the HER2 was also investigated *in vitro*. Two ovarian tumor cell lines were selected, a HER2-positive cell line (SKOV-3) and a HER2-negative cell line (OVCAR-3) (**Figure 3d**). The cells were incubated with **aza-SWIR-trastuzumab-01**, and their fluorescence signal was assessed using flow cytometry (**Figure 3e,f**). After 2 h of incubation, 60% of SKOV-3 cells were fluorescent compared to 6% of OVCAR-3 cells, demonstrating a much higher specificity of **aza-SWIR-trastuzumab-01** towards cells expressing the HER2 receptor (*i.e.* SKOV-3 cells). Additionally, a confocal microscopy experiment showed **aza-SWIR-trastuzumab-01** fluorescence signal within SKOV-3 cells, while the labeled antibody did not accumulate into the OVCAR-3 cells (**Figure 3g,h**). This experiment confirmed the previous results, and suggested that **aza-SWIR-trastuzumab-01** is internalized into cells expressing HER2. As a control, the internalization of SWIR-WAZABY-01 was similar in both cell types (**Figure S9**).

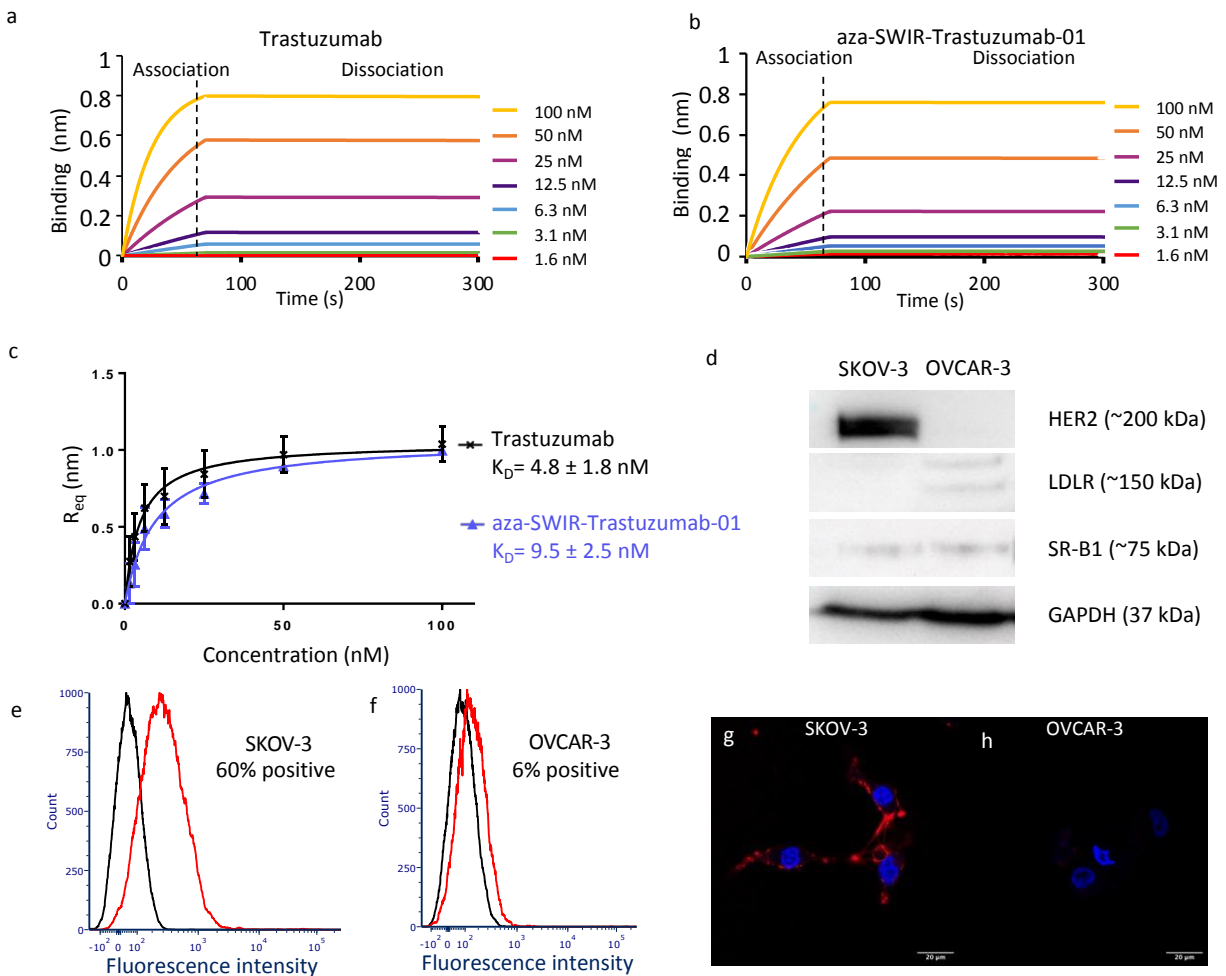


Figure 3: Assessment of **aza-SWIR-trastuzumab-01 affinity to HER2 in solution (a-c) and *in vitro* (e-h).** (a-b) Association/dissociation curves representing the interaction between free trastuzumab (a) or **aza-SWIR-trastuzumab-01** (b) (different concentrations: 1.6 to 100 nM) and HER2 proteins (coated on the biosensor), obtained using biolayer

interferometry on an Octet Red96 system. (c) K_D determination from standard curve of free trastuzumab ($K_D = 4.8 \text{ nM} \pm 1.8 \text{ nM}$) and **aza-SWIR-trastuzumab-01** ($K_D = 9.5 \text{ nM} \pm 2.5 \text{ nM}$). (d) HER2 and lipoprotein receptors (LDLR, SR-BI) expression in SKOV-3 and OVCAR-3 cells, assessed by western blotting of whole cell extracts. GAPDH served as a loading and transfer control. (e-f) Flow cytometry histograms of SKOV-3 (e) and OVCAR-3 cells (f) incubated (red lines) or not (black lines) with **aza-SWIR-trastuzumab-01**, with the percentage of fluorescently labeled cells indicated. (g-h) Confocal images of SKOV-3 (g) and OVCAR-3 (h) cells incubated with **aza-SWIR-trastuzumab-01** for 2 h. The **aza-SWIR-trastuzumab-01** fluorescence signal is indicated in red, and mainly observed in SKOV-3 cells, and the nucleus is counterstained in blue. Scale bars represent 20 μm .

Following the successful results obtained *in vitro*, the targeting potential of **aza-SWIR-trastuzumab-01** was investigated *in vivo* (**Figure 4a**). As a control, mice bearing subcutaneous SKOV-3 and OVCAR-3 tumors were administered with the free **SWIR-WAZABY-01**. Similar to previously reported data for LDL receptor-negative tumors, no significant tumor accumulation was observed, in both SKOV-3 and OVCAR-3 tumors, at any timepoint. Indeed, as previously described, **SWIR-WAZABY-01** is carried in the blood stream *via* lipoproteins, allowing a massive cell uptake through the lipoprotein receptors, LDLR and SR-B1¹⁴. Therefore, the weak tumor accumulation in SKOV-3 and OVCAR-3 models could be explained by the low or absent lipoproteins receptor expression in those tumors (**Figure 3d**), that limit the accumulation of **SWIR-WAZABY-01** fluorophore carried by lipoproteins. On the contrary, the administration of the HER2 targeting **aza-SWIR-trastuzumab-01** to mice bearing HER2-positive SKOV-3 tumors lead to a high fluorescence signal for visualizing tumors in the SWIR region, and an increasing tumor/skin fluorescence ratio over time reaching a high value of 5.5 after 72 h of administration (**Figure 4b**), as reported with other fluorescent antibodies¹⁶. As expected, the **aza-SWIR-trastuzumab-01** did not accumulate in OVCAR-3 HER2-negative tumors, with a poor tumor/skin fluorescence ratio close to 1.5 (**Figure 4b**). These findings demonstrate **aza-SWIR-trastuzumab-01** maintained a high affinity towards HER2-positive tumors *in vivo*, and possessed the ability to vectorize the **SWIR-WAZABY-01** fluorophore into HER-2 expressing tumors, despite their low expression level of lipoprotein receptors. It is worth noting that the injected dose of free **SWIR-WAZABY-01** fluorophore was 8 times higher compared to the amount of **SWIR-WAZABY-01** grafted onto the antibodies (20 nmol *versus* 2.5 nmol of dye, respectively). Therefore, a specific imaging of HER2-expressing tumors was performed using **aza-SWIR-trastuzumab-01**, with very low injected doses of fluorophore.

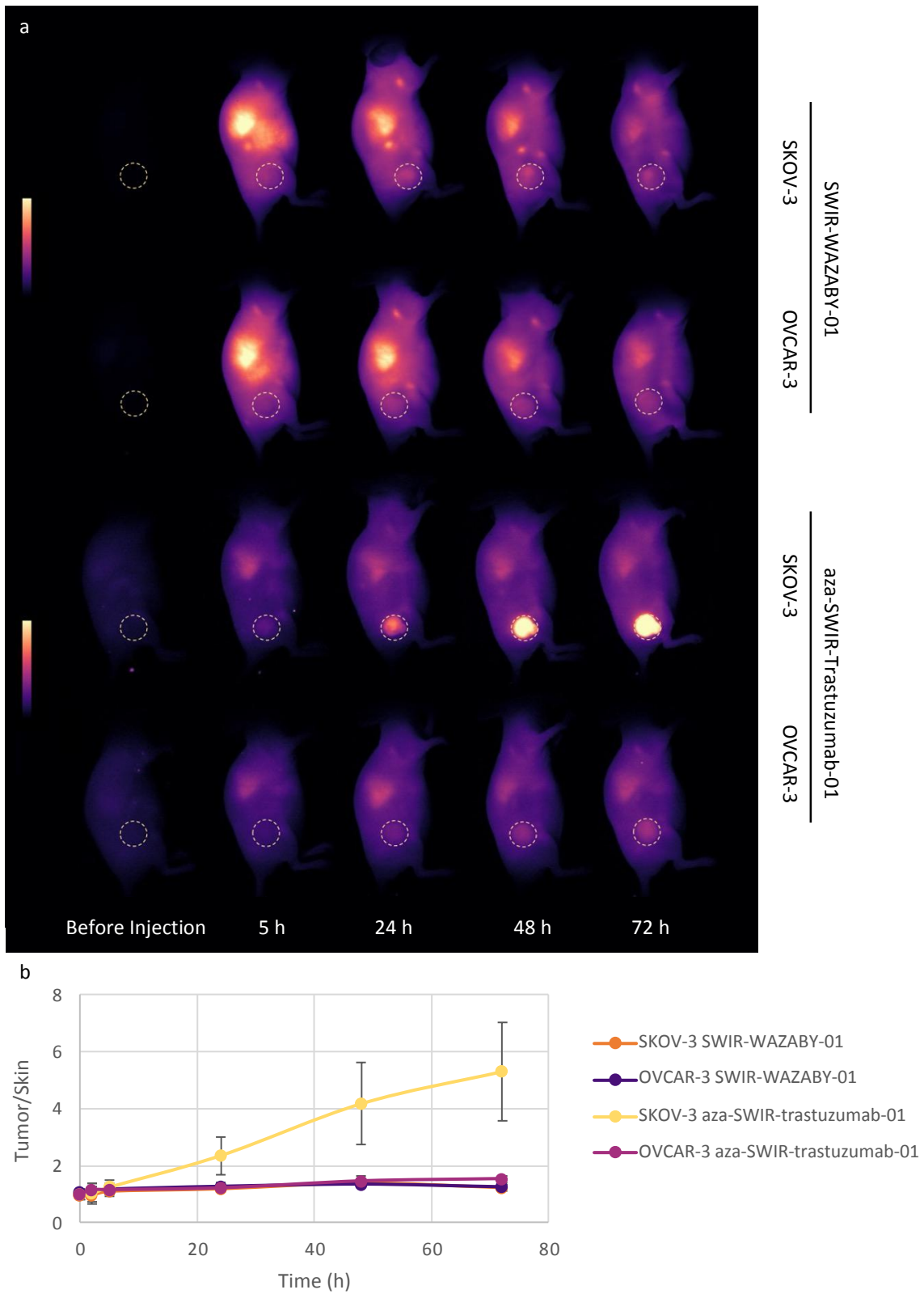


Figure 4: Assessment of aza-SWIR-trastuzumab-01 affinity to HER2 *in vivo*. (a) NIR-II fluorescence images of mice bearing subcutaneous SKOV-3 or OVCAR-3 tumors, before and at 5, 24, 48 and 72 h post intravenous administration

of **SWIR-WAZABY-01** or **aza-SWIR-trastuzumab-01**. Tumors are indicated by dashed circles. Images were acquired using 100 ms of laser exposure using a LP1064 filter. (b) Tumor/Skin ratios calculated from the *in vivo* NIR-II fluorescence images of the mice in (a) (n=3/condition).

Comparison between dyes

In order to increase the donor character in the “south” positions of the aza-BODIPYs and study the influence of this modification on the NIR-II brightness of the dye, another NIR-II emitting aza-BODIPY fluorophore was synthesized, named **SWIR-WAZABY-02**, for which the -OMe were replaced by -NMe₂ groups (Figure 5). **SWIR-WAZABY-02** and **aza-BCN-02** were synthesized following a similar synthetic pathway as described before for **SWIR-WAZABY-01** and **aza-BCN-01** (Scheme S1). **SWIR-WAZABY-02** (Scheme S2, Figures S10-16) possessed a higher quantum yield compared to **SWIR-WAZABY-01** (Table 1), in the same range as compared to reported NIR-II organic compounds²². Even though its fluorescence maximum emission peak is blue shifted compared to **SWIR-WAZABY-01** (Figure 6a), **SWIR-WAZABY-02** still possess an emission tail in the NIR-II region, and is brighter in the NIR-II window, in solution and also when diluted in serum, as demonstrated in Figure 6b.

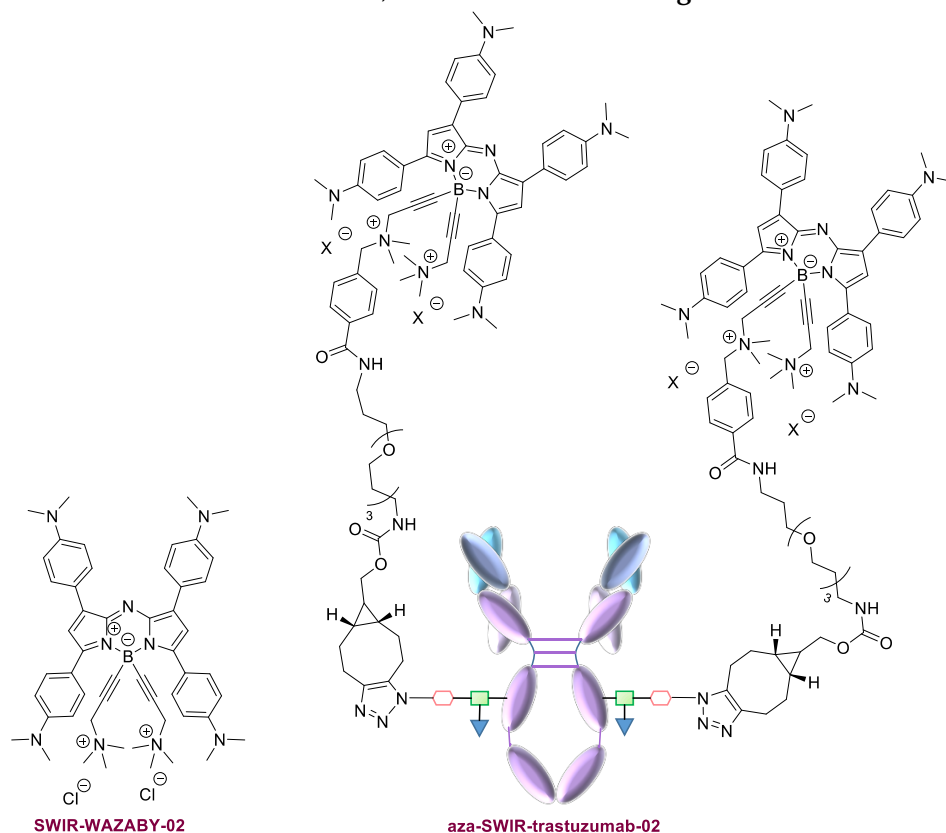


Figure 5: Structures of **SWIR-WAZABY-02** and the resulting bioconjugate **aza-SWIR-trastuzumab-02**.

Compound	In DMSO					In PBS with 10% serum	
	ϵ ($M^{-1}cm^{-1}$)	Stokes Shift (cm^{-1})	λ_{max} (nm)	λ_{em} (nm)	Φ (%)	λ_{max} (nm)	λ_{em} (nm)
SWIR-WAZABY-01	38000	2739	780	992	0.3	746	867
SWIR-WAZABY-02	73000	831	820	880	1.1	802	846

Table 1: Photophysical properties of the non-conjugated SWIR-WAZABY-01 and SWIR-WAZABY-02 dyes/fluorophores at 25 °C in DMSO or in PBS with 10% serum. Using IR 125 as reference ($\Phi_F = 0.132$ in ethanol)²³ with $\lambda_{exc} = 680$ nm.

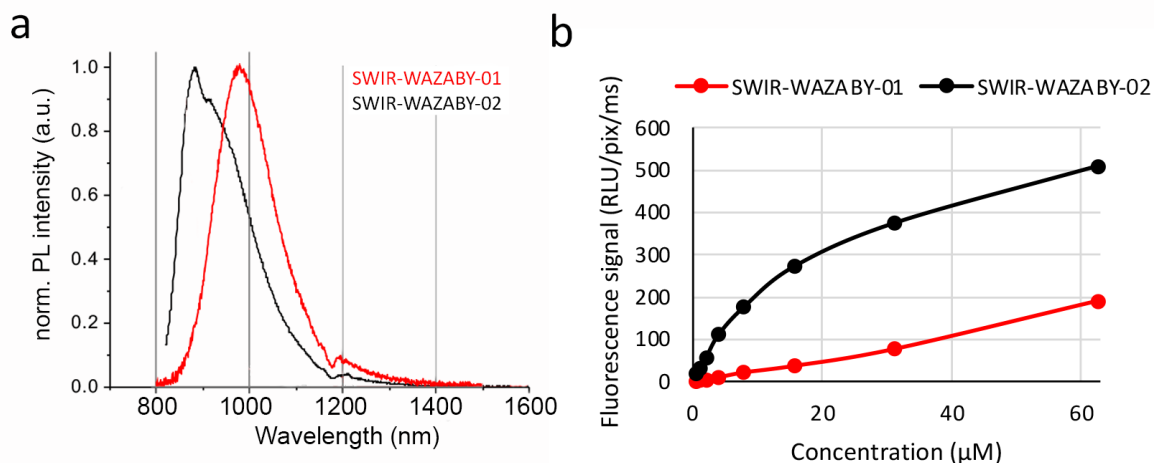


Figure 6: (a) Normalized emission spectra of SWIR-WAZABY-01 (red) and SWIR-WAZABY-02 (black) in DMSO. $\lambda_{excitation} = 806$ nm for SWIR-WAZABY-01 and 808 nm for SWIR-WAZABY-02. (b) Quantification of SWIR-WAZABY-01 and SWIR-WAZABY-02 NIR-II fluorescence signal following serial dilution in blood serum.

Similar to SWIR-WAZABY-01, SWIR-WAZABY-02 was investigated *in vivo*. SWIR-WAZABY-02 was injected into mice bearing SKOV-3 and OVCAR-3 tumors either alone without targeting moiety, or as a trastuzumab bioconjugate, *i.e.*, aza-SWIR-trastuzumab-02 (Scheme S3). Aza-SWIR-trastuzumab-02 was synthesized using the same experimental conditions as aza-SWIR-trastuzumab-01 and a DOL of 1.4 was obtained (Figure S7b). *In vivo*, SWIR-WAZABY-02 did not label SKOV-3 and OVCAR-3 tumors, similarly to SWIR-WAZABY-01 (Figure S17), whereas aza-SWIR-trastuzumab-02 labeled HER2-positive SKOV-3 tumors and not HER2-negative OVCAR-3 tumors, in a similar manner to aza-SWIR-trastuzumab-01 (Figure S17).

Comparing aza-SWIR-trastuzumab-01 to aza-SWIR-trastuzumab-02, similar tumor accumulation kinetics were observed (Figure 7a). However, aza-SWIR-trastuzumab-02 showed a brighter SWIR fluorescence signal with reduced injection dose of fluorophore at similar exposure timepoints (1 nmol *versus* 2.5 nmol of dye, respectively). The biodistribution profiles were also studied, and the brighter aza-SWIR-trastuzumab-02 possessed higher accumulation in the tumor and liver, and less accumulation in the other organs (Figure 7b; see also Figure S18). As a consequence, the tumor-to-healthy tissues fluorescence ratios were more favorable

for **aza-SWIR-trastuzumab-02** when compared with **aza-SWIR-trastuzumab-01** (Figure 7c). In particular, tumor/muscle (23.3 vs. 6.9, respectively), tumor/skin (7.6 vs. 3, respectively), and tumor/fat (26.8 vs. 7.3, respectively) ratios were all indicating the superiority of **aza-SWIR-trastuzumab-02** for tumor imaging.

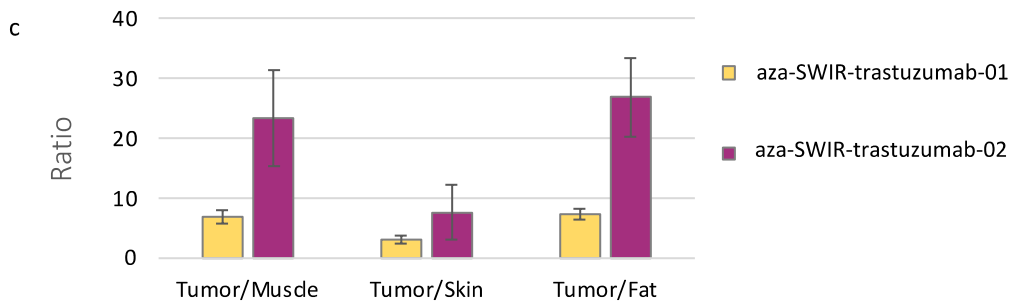
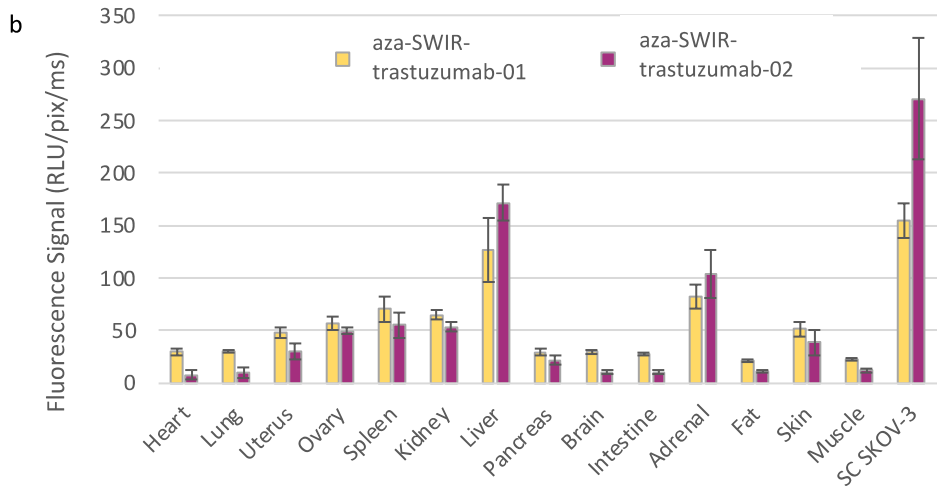
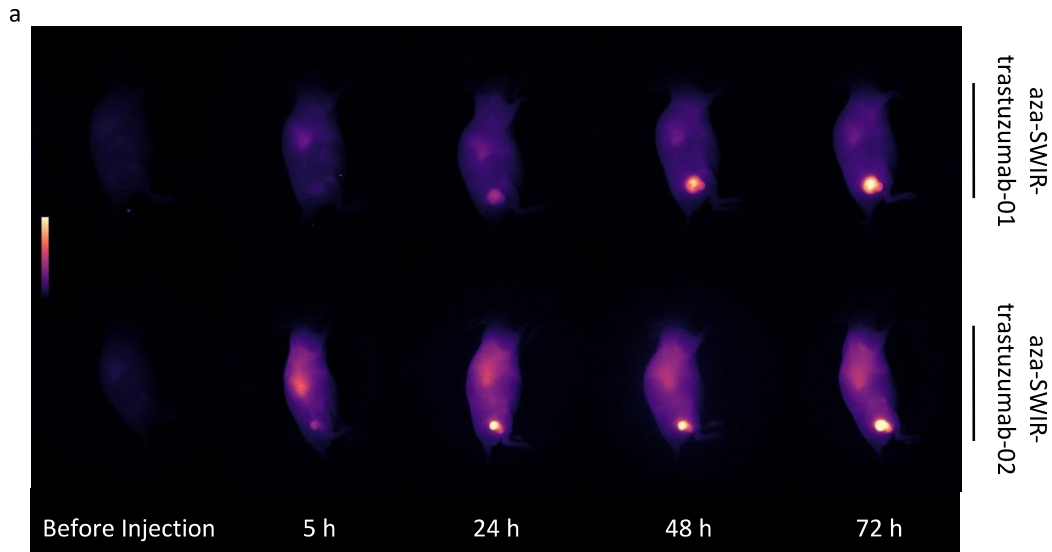


Figure 7: Comparison between aza-SWIR-trastuzumab-01 and aza-SWIR-trastuzumab-02. (a) NIR-II fluorescence images of mice bearing subcutaneous SKOV-3 before and at 5, 24, 48 and 72 h post intravenous administration of **aza-SWIR-trastuzumab-01** or **aza-SWIR-trastuzumab-02**. Images were acquired at 100 ms of laser exposure with a LP1064 filter. (b) *Ex-vivo* biodistribution of **aza-SWIR-trastuzumab-01** and **aza-SWIR-trastuzumab-02** in mice bearing subcutaneous SKOV-3 tumors 72 h post injection. (c) Tumor/Muscle, Tumor/Skin and Tumor/Fat ratios calculated from the organs fluorescence in (b), measured 72 h post injection.

In addition, such distribution profile and optical properties were observed in two different sub-optical windows, *i.e.* 1064-1700 nm and 1250-1700 nm (*Figure 8*). This latter optical window notably permits the reduction of the tissue's autofluorescence and scattering¹¹. While some discrepancies were observed between the different optical conditions, no statistical differences were found between the measured tumor/skin ratios. The fluorescence intensity adjustment allowed to observe tumors with relevant contrast as early as 5 h post-injection when measured at 1064-1700 nm, or after 24 h when measured at 1250-1700 nm.

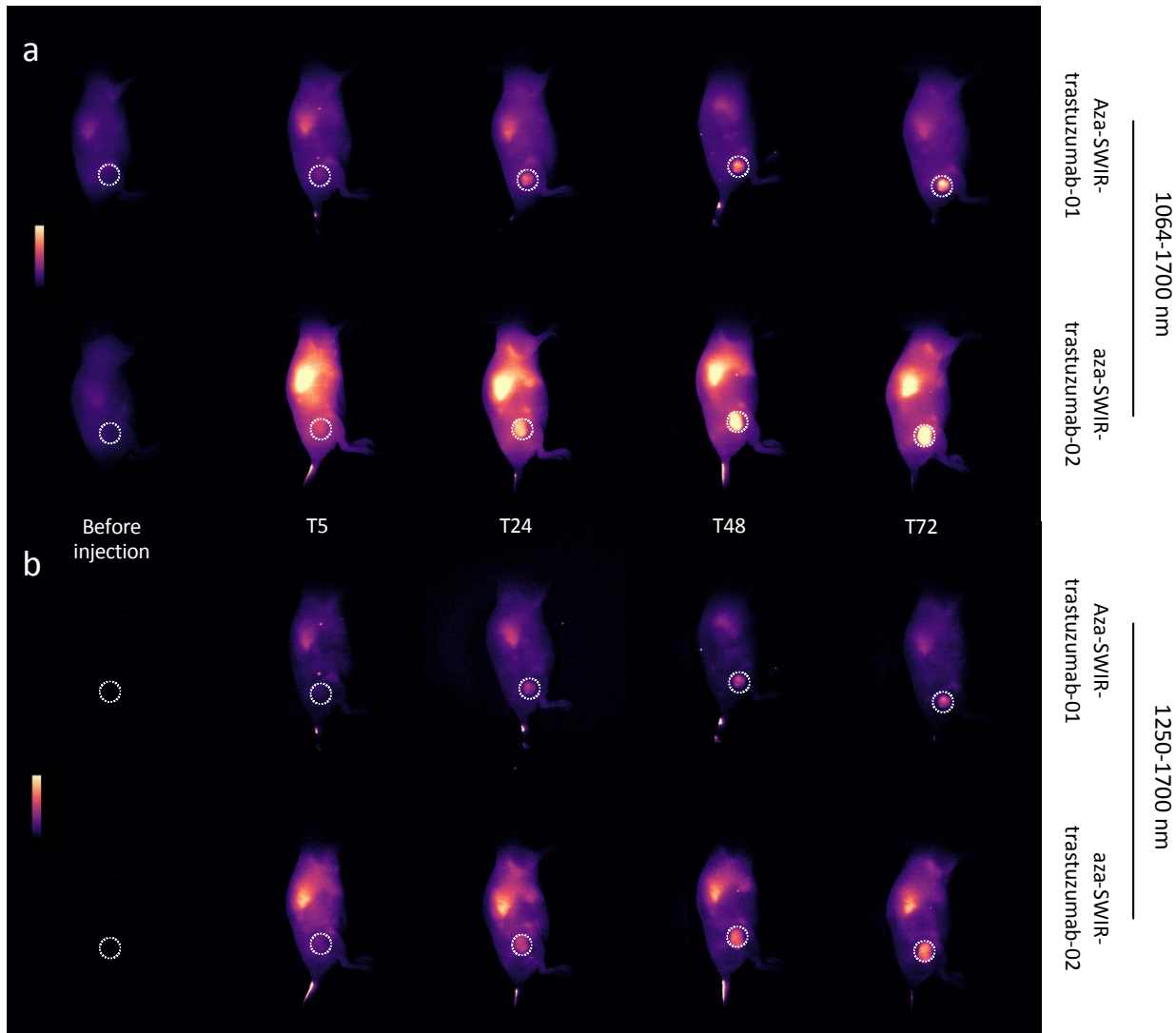


Figure 8: Comparison between aza-SWIR-trastuzumab-01 and aza-SWIR-trastuzumab-02 at 1064 and 1250 nm. (a-b) NIR-II fluorescence images of mice bearing subcutaneous SKOV-3 before and at 5, 24, 48 and 72 h post intravenous administration of **aza-SWIR-trastuzumab-01** or **aza-SWIR-trastuzumab-02**. Images were acquired at 100 ms of laser exposure for (a) 1064-1700 nm (image color scale 500-12000) and (b) 500 ms of laser exposure for 1250-1700 nm (image color scale 500-5000).

Conclusion

To conclude, we reported and demonstrated a specific bioconjugation technique to couple water-soluble NIR-II emitting aza-BODIPY dyes to trastuzumab, an approved anticancer therapeutic antibody. These vectorized aza-BODIPYs are promising fluorescent dyes for molecular imaging and FGS applications, because of their strong photostability and fluorescence properties. We showed that the resulting bioconjugates maintained prolonged fluorescence stability and affinity towards HER2 receptors both in solution and *in vitro*. *In vivo*, the bioconjugated dyes conserved their fluorescence properties and allowed the specific labeling of HER2-positive ovarian tumors. The obtained tumor/muscle ratios demonstrated the potential of the NIR-II bioconjugated dyes for NIR-II fluorescence-guided surgery. This bioconjugation process employed here should be useful for coupling other aza-BODIPYs to antibodies, thus allowing the targeting of a wider range of tumors with unique fluorescence properties.

Material and Methods:

The chemical synthesis will be described in the supplementary information; all the HPLC are provided in this section (Figures S1-S6 and Figure S10-16).

Reagents and chemicals for synthesis:

Reactions were carried out in analytical reagent grade solvents from Carlo Erba under normal atmosphere. Non-stabilized dry solvents were purchased from Carlo Erba and dried using a MB-SPS-800 (MBraun) or PureSolv-MD-5 (Inert®). All reagents purchased from SigmaAldrich™, Thermo Fisher Scientific™ or ACROS Organics™ were used as received without further purification. Reactions were monitored by thin-phase chromatography and RP-HPLC-MS. Analytical thin-phase chromatography was performed using Merck 60 F254 silica gel (precoated sheets, 0.2 mm thick). Column chromatography was carried out using silica gel (SigmaAldrich; 40-63 μm 230-400 mesh 60Å). Purity was determined from HPLC analysis and was >95 % for all the injected compounds.

Photophysical studies:

Absorbance measurements were recorded on a UV-Vis-NIR spectrophotometer Cary5000 between 300 and 1200 nm. Steady-state photoluminescence spectra were measured from 700 to

1500 nm with a calibrated FSP 920 (Edinburgh Instruments, Edinburgh, United Kingdom) spectrofluorometer equipped with a nitrogen-cooled PMT R5509P. Relative measurements of photoluminescence QYs ($\Phi_{f,x}$) were performed using the dye IR125 dissolved in dimethylsulfoxide (DMSO) as reference. The QY of this dye was previously determined absolutely to $\Phi_{f,st} = 0.23$. The relative QY were calculated according to the formula of Demas and Crosby, see equation below.

$$\Phi_{f,x} = \Phi_{f,st} \frac{F_x f_{st}(\lambda_{ex,st}) n_x^2(\lambda_{ex,x})}{F_{st} f_x(\lambda_{ex,x}) n_{st}^2(\lambda_{ex,st})}$$

The subscripts x, st, and ex denote sample, standard, and excitation respectively. $f(\lambda_{ex})$ is the absorption factor, F the integrated spectral fluorescence photon flux, and n the refractive index of the solvents used. All spectroscopic measurements were done in a 1 cm quartz cuvettes from Hellma GmbH at room temperature using air-saturated solutions.

Photophysical analysis for these compounds were performed at the Federal Institute for Materials Research and Testing (BAM) Division Biophotonics in Berlin (Germany).

Trastuzumab modification:

Trastuzumab modification was carried out using the GlyCLICK® technology marketed by Genovis®. It consists of two steps. Step one involves the hydrolysis of the bonds between the two *N*-acetylglucosamines using EndoS, an enzyme belonging to the endoglycosidase family. This reaction was carried out for one hour, at room temperature, in TBS and at pH = 7.5, resulting in a deglycosylated antibody. The second step involves a second enzyme, GalT, which belongs to the nucleotidyltransferase (galactosyltransferase) family. GalT allows the transfer of an azide-bound galactose from UDP-GalN_{az} onto the deglycosylated antibody. This reaction was carried out overnight, at 25 °C, in tris buffer saline (TBS) and at pH = 7.5. The modified antibody can now be engaged in a SPAAC reaction with **aza-BCN-01/ aza-BCN-02** dye.

Bioconjugation:

aza-BCN-01 dye (14 equivalents) was incubated with 1 mg of trastuzumab-N₃ in PBS, at pH = 7.4, at 25 °C, for 16 h. The reaction crude was then purified by FPLC and the solution was concentrated to determine the DOL by MALDI-TOF.

aza-BCN-02 dye (20 equivalents) was incubated per trastuzumab-N₃ antibody. The reaction was performed in PBS overnight, at pH = 7.4 and at 25 °C. A PD-10 column size exclusion column was used to purify the bioconjugate. PD-10 allows the separation of high molecular weight compounds, the bioconjugated antibody, from low molecular weight compounds, the free dye. Two columns were used to ensure that all the free dyes had been removed. The recovered sample was then concentrated on Amicon® and was analyzed using MALDI-TOF to determine the DOL.

Antibody Stability:

The stability of **Aza-SWIR-trastuzumab-01** was determined using the following procedure. **Aza-SWIR-trastuzumab-01** was diluted in PBS at 1 mg/mL, then it was incubated in murine or human sera for 24 h, 48 h or 72 h, at 0.5 mg/mL. Incubations were carried out at 37 °C, in the dark and under gentle agitation. Trastuzumab incubated in sera for 72 h served as a control. Each antibody sample was then diluted to 0.125 mg/mL in Laemmli buffer under either reducing (in the presence of dithiothreitol (DTT) and heating at 95 °C for 5 minutes) or non-reducing (without DTT) conditions, after which they were separated on a sodium dodecyl sulfate polyacrylamide gel electrophoresis (SDS-PAGE). For each experimental condition, the equivalent of 1.5 µg of antibody was deposited on a 10% acrylamide gel, and a 1.5 h migration at 100 V was performed. Following migration, the fluorescence of the gel was monitored using ChemiDoc® MP imaging device (BioRad®) with an IRdye800CW filter. Finally, the gels were stained with Coomassie blue for 1 h, and visualized on a Chemidoc XRS + analyzer (Bio-Rad), to detect the proteins.

Biolayer Interferometry:

The affinity of **Aza-SWIR-trastuzumab-01** or native trastuzumab antibodies to HER-2 was determined using biolayer interferometry (BLI), on an OctetRed96e instrument (FortéBio). HER-2 was first biotinylated with 5 equiv. of biotin (biotin-PEG4-NHS EZkit, Pierce) according to the manufacturer's instructions. Streptavidin-coated biosensors were then dipped into the wells containing biotinylated HER-2 resulting in functionalized biosensors. To study the trastuzumab-HER-2 interaction, association and dissociation phases were determined by dipping the functionalized biosensors (Accrobiosystem) into wells containing different concentrations of trastuzumab or **Aza-SWIR-trastuzumab-01** (1.6 to 100 nM), followed by wells containing PBS. Finally, KD was determined using the Octet software (version 3.1, FortéBio, Menlo Park, CA, USA) with a 1:1 stoichiometry model.

Cell Lines and Culture:

Human ovarian adenocarcinoma cell lines, SKOV-3 and OVCAR-3, were obtained from the European Collection of Authenticated Cell Cultures (ECACC, French authorization CODECOH DC-2020-4226). The cell lines were cultured in a 37 °C humidified environment containing 5% CO₂, and in DMEM media supplemented with 10% heat-inactivated fetal bovine serum.

Flow Cytometry:

SKOV-3 and OVCAR-3 cells were harvested, washed and incubated with **aza-SWIR-trastuzumab-01** for 2 h at 37 °C. The cells were then rinsed, fixed with PFA 4% and analyzed using LSRII (BD-Biosciences). At least, 10000 events were recorded and APC-Cy7 excitation

settings were used, without pass-band filter for optimal collection (LP 755 nm). Data analysis was performed using FCS Express Flow (V7- Pro RUO) software.

Confocal Microscopy:

SKOV-3/OVCAR-3 cells (n = 50,000) were plated on LabTek chamber I and kept at 37 °C in 5% CO₂. After 24 h of adhesion, the cells were washed and incubated with 36 mg/L of **aza-SWIR-trastuzumab-01** compound solution (*i.e.* 0.5 μM of fluorophore) diluted in cell culture medium, for 2 h. The cells were then washed and counterstained with Hoechst 33342 (1 μM). Fluorescence microscopy images were acquired using a confocal laser-scanning microscope (LSM 710 Carl Zeiss, Jena, Germany) in APD live mode. Plan x63 objective was used. Fluorescent signal was obtained with a 25% 633 nm excitation laser, and a collection wavelength > 650 nm (confocal section 1.5 μm). Images were processed using Fiji software. The experiments were performed at the MicroCell (Optical Microscopy-Cell Imaging, A. Grichine & M. Pyzet) platform, IAB Grenoble.

Western blot

SKOV-3 and OVCAR-3 tumor cells cultured in 2D were harvested, washed with PBS, lysed and their protein content was quantified using Micro BCA™ Protein Assay Kit (Thermo Fisher Scientific). 40 μg of protein/cell line was loaded into a 12% polyacrylamide gel. Following migration/electrophoresis, the proteins were transferred into an activated PVDF (polyvinylidene difluoride) membrane (#10600023, Amersham). The membrane was then blocked at RT in 5% milk for 1 h, and incubated with primary antibodies overnight at 4 °C: anti-LDL receptor antibody (1/1000, Abcam [EP1553Y] (ab52818)), anti-scavenging receptor SR-BI antibody (1/2000, Abcam [EPR20190] (ab217318)), anti-HER2 antibody (1/1000, cell signaling #4290) and anti-GAPDH antibody (1/1000, SC-365062, Santa Cruz Biotechnology) serving as loading and transfer control. The membrane was then incubated with the secondary antibodies, anti-mouse/rabbit-horseradish peroxidase HRP (1/2000, #7076S, Cell Signaling Technology) for 1 h, at RT. The proteins (LDLR/SR-B1/HER2/GAPDH) were finally revealed using Clarity Western ECL Substrate (Bio-Rad), and western blot imaging was performed using Fusion FX (Vilber).

***In vivo* NIR-II imaging**

All animal experiments were performed in accordance with national legislation, and with the approval of the institutional and national (Ministère de l'Enseignement Supérieure et de la Recherche) animal ethics committees (APAFIS#8782-2017032813328550), and were performed according to the Institutional Animal Care and Use Committee of Grenoble Alpes University and the Federation of European Animal Science Associations. These experiments were carried out within the small animal imaging platform *Optimal* (Dr V. Jossierand), IAB Grenoble. Female NMRI nude mice (6-week-old) (Janvier Labs, Le Genest-Saint Isle, France) were subcutaneously

injected on their right flank with either 10 million of human ovarian adenocarcinoma SKOV-3 cancer cells, or 8 million of human ovarian adenocarcinoma OVCAR-3 cancer cells. Following tumor growth, SKOV-3 and OVCAR-3 bearing mice were intravenously injected in their tail vein with either 100 μ L of 200 μ M **SWIR-WAZABY-01** or **SWIR-WAZABY-02** solution diluted in PBS, or with 100 μ L of 200 μ g **aza-SWIR-trastuzumab-01** or 100 μ g of **aza-SWIR-trastuzumab-02** (n=3/condition). Whole-body NIR-II fluorescence imaging was performed before and at 5, 24, 48, and 72 h after administration. At 72 h, the mice were euthanized and their organs were sampled for *ex-vivo* fluorescence imaging. Acquired images were analyzed using Fiji software, and semi-quantitative fluorescence data were obtained by drawing regions of interest (ROI) around the organs. NIR-II fluorescence imaging was performed using a Princeton camera 640ST (900–1700 nm) coupled to a laser excitation source of $\lambda = 808$ nm (50 mW/cm²). A short-pass excitation filter at 1000 nm (Thorlabs), a long-pass filter LP1064 nm (Semrock), and a long-pass filter LP1250 nm (Semrock) were added to the NIR-II camera. A 25 mm lens with 1.4 aperture (Navitar) was used to focus on the mice.

Abbreviations

APD: Avalanche Photo Diode; APC-Cy7: Allophycocyanin-Cyanin7; Aza-BODIPY: Aza-boron-dipyrromethene; BLI: bilayer interferometry; BODIPY: boron-dipyrromethene; DOL: degree of labeling; FGS: fluorescence guided surgery; FPLC: fast protein liquid chromatography; GAPDH: glyceraldehyde-3-phosphate dehydrogenase; HBTU: 2-(1H-benzotriazol-1-yl)-1,1,3,3-tetramethyluronium hexafluorophosphate; HER2: human epidermal growth factor receptor 2; HRP: horseradish peroxidase; K_D: Dissociation constant; LDLR: Low Density Lipoprotein receptor; LP1064 nm: Long-pass 1064 nm; NIR: Near Infrared; QDots: Quantum Dots; QYs: Quantum Yields; RP-HPLC-MS: Reverse phase high-performance liquid chromatography-mass spectrometry; SDS-PAGE: sodium dodecyl sulfate polyacrylamide gel electrophoresis; SPAAC: strain-promoted alkyne-azide cycloaddition; SR-BI: Class B Scavenger receptor B1; SWIR: Short Wave Infrared; TBS: tris buffer saline; TOTA: 4,7,10-trioxa-13-tridecanamine; WAZABY: Water-Soluble aza-BODIPY.

Acknowledgements

The researchers gratefully acknowledge the following funds related to this paper: FRM ECO201806006861, Oncostarter project of the cancerôle CLARA (Agnostic project), France Life Imaging (Thera-BODIPY), GEFLUC Grenoble Dauphiné Savoie, the French National Research Agency (JCJC ANR-18-CE18-0012, Ligue Contre le Cancer AURA and Grand-Est-BFC), and the SATT Linksum Grenoble Alpes for the project FLUO-NIR-2. GDR AIM is acknowledged for fruitful discussion. M.-J. Penouilh and Q. Bonnin are gratefully acknowledged for HR-MS analysis, M. Heydel for the ionic chromatography, M. Picquet for NMR analyses, A. Romieu and V. Goncalves are acknowledged for the TOTA-Boc and (1R,8S,9S)-bicyclo[6.1.0]non-4-y,-9-ylmethyl N-succinimidyl carbonate compounds respectively.

Supporting Information

In this section, additional methods are provided for the following: NMR Spectroscopy; Mass Spectrometry; Analytical HPLC; Semi-preparative HPLC; MALDI-TOF; Ion Chromatography; Detailed and characterization of intermediated compounds 1 to 3, aza-SWIR-02, aza-propargyl-02, SWIR-WAZABY-02, aza-acid-01, aza-acid-02, aza-TOTA-01, aza-TOTA-02, aza-squaramate-01, aza-BCN-01, aza-BCN-02; Synthetic pathway of the trastuzumab-site specific conjugated NIR-II emitting aza-BODIPY, aza-SWIR-trastuzumab-01; Synthetic pathways of SWIR-WAZABY-02 and aza-SWIR-trastuzumab-02; UV-Vis spectrum of aza-SWIR-02, SWIR-WAZABY-02, aza-squaramate-01, aza-BCN-01 and aza-BCN-02 in water at 25 °C; Chromatogram obtained in LC-MS of SWIR-WAZABY-02, aza-acid-01, aza-acid-02, aza-TOTA-01, aza-TOTA-02, aza-squaramate-01, aza-BCN-01, and aza-BCN-02; Determining trastuzumab degree of labeling (DOL) in aza-SWIR-trastuzumab compounds; Assessment of aza-SWIR-trastuzumab-01 stability in human serum solution; Confocal images of cells incubated with SWIR-WAZABY-01; Assessment of aza-SWIR-trastuzumab-02 affinity to HER2 in vivo; and Representative ex-vivo fluorescence imaging of organs of the Figure 7.

Corresponding authors

Christine Goze, Institut de Chimie Moléculaire de l'Université de Bourgogne, Université de Bourgogne, CNRS UMR 6302, 21078 Dijon, France. orcid.org/0000-0002-3484-3837; christine.goze@u-bourgogne.fr

Lucie Sancey, Université Grenoble Alpes, INSERM U1209, CNRS UMR 5309, Institute for Advanced Biosciences (IAB), 38000 Grenoble, France. [Orcid.org/0000-0002-0084-3775](https://orcid.org/0000-0002-0084-3775); Lucie.sancey@univ-grenoble-alpes.fr

Competing interests

A. G., G. K., B. B., X. L.-G., J.-L. C., F. D., E. B., C. G., L. S. have a patent to declare, related to the fluorescent aza- BODIPY (EP19315089.3/WO2021/023731). The other authors have declared that no competing interest exists.

References

(1) Randall, L. M.; Wenham, R. M.; Low, P. S.; Dowdy, S. C.; Tanyi, J. L. A phase II, multicenter, open-label trial of OTL38 injection for the intra-operative imaging of folate receptor-alpha

positive ovarian cancer. *Gynecol Oncol* **2019**, *155* (1), 63-68. DOI: 10.1016/j.ygyno.2019.07.010 From NLM.

(2) Bristow, R. E.; Tomacruz, R. S.; Armstrong, D. K.; Trimble, E. L.; Montz, F. J. Survival effect of maximal cytoreductive surgery for advanced ovarian carcinoma during the platinum era: a meta-analysis. *J Clin Oncol* **2002**, *20* (5), 1248-1259. DOI: 10.1200/jco.2002.20.5.1248 From NLM.

(3) du Bois, A.; Reuss, A.; Pujade-Lauraine, E.; Harter, P.; Ray-Coquard, I.; Pfisterer, J. Role of surgical outcome as prognostic factor in advanced epithelial ovarian cancer: a combined exploratory analysis of 3 prospectively randomized phase 3 multicenter trials: by the Arbeitsgemeinschaft Gynaekologische Onkologie Studiengruppe Ovarialkarzinom (AGO-OVAR) and the Groupe d'Investigateurs Nationaux Pour les Etudes des Cancers de l'Ovaire (GINECO). *Cancer* **2009**, *115* (6), 1234-1244. DOI: 10.1002/cncr.24149 From NLM.

(4) Vahrmeijer, A. L.; Hutteman, M.; van der Vorst, J. R.; van de Velde, C. J.; Frangioni, J. V. Image-guided cancer surgery using near-infrared fluorescence. *Nat Rev Clin Oncol* **2013**, *10* (9), 507-518. DOI: 10.1038/nrclinonc.2013.123 From NLM. Tipirneni, K. E.; Warram, J. M.; Moore, L. S.; Prince, A. C.; de Boer, E.; Jani, A. H.; Wapnir, I. L.; Liao, J. C.; Bouvet, M.; Behnke, N. K.; et al. Oncologic Procedures Amenable to Fluorescence-guided Surgery. *Ann Surg* **2017**, *266* (1), 36-47. DOI: 10.1097/sla.0000000000002127 From NLM.

(5) van Dam, G. M.; Themelis, G.; Crane, L. M.; Harlaar, N. J.; Pleijhuis, R. G.; Kelder, W.; Sarantopoulos, A.; de Jong, J. S.; Arts, H. J.; van der Zee, A. G.; et al. Intraoperative tumor-specific fluorescence imaging in ovarian cancer by folate receptor- α targeting: first in-human results. *Nat Med* **2011**, *17* (10), 1315-1319. DOI: 10.1038/nm.2472 From NLM.

(6) Clinicaltrials.gov. ELUCIDATE: Enabling LUng Cancer IDentification Using folATE Receptor Targeting. **2020**, *NCT04241315*. Clinicaltrials.gov. SGM-101 in Locally Advanced and Recurrent Rectal Cancer (SGM-LARRC). **2020**, *NCT04642924*.

(7) Hong, G.; Antaris, A. L.; Dai, H. Near-infrared fluorophores for biomedical imaging. *Nat Biomed Eng* **2017**, *1* (1), 0010. DOI: 10.1038/s41551-016-0010. Musnier, B.; Henry, M.; Vollaire, J.; Coll, J. L.; Usson, Y.; Josserand, V.; Le Guevel, X. Optimization of spatial resolution and scattering effects for biomedical fluorescence imaging by using sub-regions of the shortwave infrared spectrum. *J Biophotonics* **2021**, *14* (2), e202000345. DOI: 10.1002/jbio.202000345.

(8) Wang, F.; Qu, L.; Ren, F.; Baghdasaryan, A.; Jiang, Y.; Hsu, R.; Liang, P.; Li, J.; Zhu, G.; Ma, Z.; et al. High-precision tumor resection down to few-cell level guided by NIR-IIb molecular fluorescence imaging. *Proc Natl Acad Sci U S A* **2022**, *119* (15), e2123111119. DOI: 10.1073/pnas.2123111119.

(9) Shi, H.; Huttad, L. V.; Tan, M.; Liu, H.; Chua, M. S.; Cheng, Z.; So, S. NIR-II imaging of hepatocellular carcinoma based on a humanized anti-GPC3 antibody. *RSC Med Chem* **2022**, *13* (1), 90-97. DOI: 10.1039/d1md00313e.

(10) Kurbegovic, S.; Juhl, K.; Chen, H.; Qu, C.; Ding, B.; Leth, J. M.; Drzewiecki, K. T.; Kjaer, A.; Cheng, Z. Molecular Targeted NIR-II Probe for Image-Guided Brain Tumor Surgery. *Bioconjug Chem* **2018**, *29* (11), 3833-3840. DOI: 10.1021/acs.bioconjchem.8b00669. Sun, Y.; Ding, M.; Zeng, X.; Xiao, Y.; Wu, H.; Zhou, H.; Ding, B.; Qu, C.; Hou, W.; Er-Bu, A.; et al. Novel bright-emission small-molecule NIR-II fluorophores for in vivo tumor imaging and image-guided surgery. *Chem Sci* **2017**, *8* (5), 3489-3493. DOI: 10.1039/c7sc00251c.

- (11) Carr, J. A.; Franke, D.; Caram, J. R.; Perkinson, C. F.; Saif, M.; Askoxylakis, V.; Datta, M.; Fukumura, D.; Jain, R. K.; Bawendi, M. G.; et al. Shortwave infrared fluorescence imaging with the clinically approved near-infrared dye indocyanine green. *Proc Natl Acad Sci U S A* **2018**, *115* (17), 4465-4470. DOI: 10.1073/pnas.1718917115.
- (12) Godard, A.; Kalot, G.; Pliquett, J.; Busser, B.; Le Guével, X.; Wegner, K. D.; Resch-Genger, U.; Rousselin, Y.; Coll, J. L.; Denat, F.; et al. Water-Soluble Aza-BODIPYs: Biocompatible Organic Dyes for High Contrast In Vivo NIR-II Imaging. *Bioconjug Chem* **2020**, *31* (4), 1088-1092. DOI: 10.1021/acs.bioconjchem.0c00175 From NLM.
- (13) Rappitsch, T.; S, M. B. Carbazole- and Fluorene-Fused Aza-BODIPYs: NIR Fluorophores with High Brightness and Photostability. *Chemistry* **2021**, *27* (41), 10685-10692. DOI: 10.1002/chem.202100965. Bertrand, B.; Passador, K.; Denat, F.; Bodio, E.; Salmain, M. Metal-based BODIPY derivatives as multimodal tools for life sciences. *Coord Chem Rev* **2018**, *358*, 108-124. DOI: 10.1016/j.ccr.2017.12.007.
- (14) Kalot, G.; Godard, A.; Busser, B.; Bendellaa, M.; Dalonneau, F.; Paul, C.; Le Guevel, X.; Josserand, V.; Coll, J. L.; Denat, F.; et al. Lipoprotein interactions with water-soluble NIR-II emitting aza-BODIPYs boost the fluorescence signal and favor selective tumor targeting. *Biomater Sci* **2022**. DOI: 10.1039/d2bm01271e.
- (15) Verri, E.; Guglielmini, P.; Puntoni, M.; Perdelli, L.; Papadia, A.; Lorenzi, P.; Rubagotti, A.; Ragni, N.; Boccardo, F. HER2/neu oncoprotein overexpression in epithelial ovarian cancer: evaluation of its prevalence and prognostic significance. Clinical study. *Oncology* **2005**, *68* (2-3), 154-161. DOI: 10.1159/000086958 From NLM.
- (16) Debie, P.; Van Quathem, J.; Hansen, I.; Bala, G.; Massa, S.; Devoogdt, N.; Xavier, C.; Hernot, S. Effect of Dye and Conjugation Chemistry on the Biodistribution Profile of Near-Infrared-Labeled Nanobodies as Tracers for Image-Guided Surgery. *Mol Pharm* **2017**, *14* (4), 1145-1153. DOI: 10.1021/acs.molpharmaceut.6b01053. Sampath, L.; Kwon, S.; Ke, S.; Wang, W.; Schiff, R.; Mawad, M. E.; Sevick-Muraca, E. M. Dual-labeled trastuzumab-based imaging agent for the detection of human epidermal growth factor receptor 2 overexpression in breast cancer. *J Nucl Med* **2007**, *48* (9), 1501-1510. DOI: 10.2967/jnumed.107.042234. Sano, K.; Mitsunaga, M.; Nakajima, T.; Choyke, P. L.; Kobayashi, H. In vivo breast cancer characterization imaging using two monoclonal antibodies activatably labeled with near infrared fluorophores. *Breast Cancer Res* **2012**, *14* (2), R61. DOI: 10.1186/bcr3167.
- (17) Sato, K.; Nagaya, T.; Nakamura, Y.; Harada, T.; Nani, R. R.; Shaum, J. B.; Goraka, A. P.; Kim, I.; Paik, C. H.; Choyke, P. L.; et al. Impact of C4'-O-Alkyl Linker on in Vivo Pharmacokinetics of Near-Infrared Cyanine/Monoclonal Antibody Conjugates. *Mol Pharm* **2015**, *12* (9), 3303-3311. DOI: 10.1021/acs.molpharmaceut.5b00472.
- (18) Yoon, H. Y.; Lee, D.; Lim, D. K.; Koo, H.; Kim, K. Copper-Free Click Chemistry: Applications in Drug Delivery, Cell Tracking, and Tissue Engineering. *Adv Mater* **2022**, *34* (10), e2107192. DOI: 10.1002/adma.202107192.
- (19) Pliquett, J.; Dubois, A.; Racoeur, C.; Mabrouk, N.; Amor, S.; Lescure, R.; Bettaïeb, A.; Collin, B.; Bernhard, C.; Denat, F.; et al. A Promising Family of Fluorescent Water-Soluble aza-BODIPY Dyes for in Vivo Molecular Imaging. *Bioconjug Chem* **2019**, *30* (4), 1061-1066. DOI: 10.1021/acs.bioconjchem.8b00795 From NLM.

- (20) Shibui, T.; Bando, K.; Misawa, S. High-level secretory expression, purification, and characterization of an anti-human Her II monoclonal antibody, trastuzumab, in the methylotrophic yeast *Pichia pastoris*. *Adv Biosci Biotechnol* **2013**, *04*, 640-646. DOI: 10.4236/abb.2013.45084.
- (21) Abdiche, Y.; Malashock, D.; Pinkerton, A.; Pons, J. Determining kinetics and affinities of protein interactions using a parallel real-time label-free biosensor, the Octet. *Anal Biochem* **2008**, *377* (2), 209-217. DOI: 10.1016/j.ab.2008.03.035 From NLM.
- (22) Li, B.; Zhao, M.; Feng, L.; Dou, C.; Ding, S.; Zhou, G.; Lu, L.; Zhang, H.; Chen, F.; Li, X.; et al. Organic NIR-II molecule with long blood half-life for in vivo dynamic vascular imaging. *Nat Commun* **2020**, *11* (1), 3102. DOI: 10.1038/s41467-020-16924-z. Wang, S.; Fan, Y.; Li, D.; Sun, C.; Lei, Z.; Lu, L.; Wang, T.; Zhang, F. Anti-quenching NIR-II molecular fluorophores for in vivo high-contrast imaging and pH sensing. *Nat Commun* **2019**, *10* (1), 1058. DOI: 10.1038/s41467-019-09043-x.
- (23) Rurack, K.; Spieles, M. Fluorescence quantum yields of a series of red and near-infrared dyes emitting at 600-1000 nm. *Anal Chem* **2011**, *83* (4), 1232-1242. DOI: 10.1021/ac101329h.